American Mineralogist, Volume 70, pages 279–287, 1985

Kinetic controls on pyroxene nucleation and metastable liquid lines of descent in a basaltic andesite

MICHAEL B. BAKER AND TIMOTHY L. GROVE

Department of Earth, Atmospheric and Planetary Sciences
Massachusetts Institute of Technology, Cambridge, Massachusetts 02139

Abstract

One-atmosphere dynamic crystallization experiments on a basaltic andesite show that the appearance temperatures of augite and pigeonite are sensitive to cooling rate and the amount of dissolved H_2O in the melt. With decreasing cooling rate (50° to 0.5°C/hr) the appearance temperature and Mg* [Mg* = $Mg/(Mg + Fe_{total})$] of the first crystallizing augite increases. At rates ≥ 5°C/hr the degree of undercooling at which augite first appears is identical for H_2–CO_2 and H_2–H_2O gas mixtures. At slower cooling rates pyroxene appearance is depressed to a lesser extent in the H_2–H_2O than in the H_2–CO_2 gas mixture. Under equilibrium conditions pigeonite precedes augite in the crystallization sequence; however, only in the H_2–H_2O 0.5°C/hr cooling rate experiment does pigeonite crystallize, and then it appears contemporaneously with augite. Suppression of pigeonite nucleation influences the mineral assemblage that precipitates from the basaltic andesite, and in turn the liquid line of descent followed during crystallization. The most important effect of pigeonite suppression is that metastable olivine + augite crystallization replaces the equilibrium reaction relationship olivine + liquid → pigeonite. Thermal modeling indicates that the kinetic processes reproduced by our experiments could operate within 5 m of the upper surface of thick lava flows and in crustal level dikes up to 6 m thick, and we describe well documented examples of Modoc lavas from northern California that record these non-equilibrium effects.

Introduction

This paper describes the effects of cooling rate and volatile content on the kinetics of augite and pigeonite nucleation in a basaltic andesite and compares experimentally determined metastable and equilibrium phase relations. Dynamic crystallization studies in the system MgO–SiO_2 and on lunar basalts and a basaltic achondrite have shown how cooling rate can alter crystallization sequences compared to equilibrium relationships (Kirkpatrick et al., 1983; Lofgren et al., 1974; Walker et al., 1976, 1978; Bianco and Taylor, 1977; Grove and Bence, 1977). For example, Grove and Raudsepp (1978) and Grove and Bence (1979) demonstrated that boundary curves in pseudoternary systems are displaced further from their equilibrium positions with increasing cooling rate. Walker et al. (1978) found that at cooling rates greater than 1°C/hr olivine crystallized from a basaltic achondrite even though olivine had no equilibrium crystallization field.

Recent 1-atmosphere experimental work by Grove et al. (1982, 1983) and Grove and Bryan (1983) shows that pigeonite is the first low-Ca pyroxene to crystallize from most basaltic melts. Pigeonite is also the first pyroxene predicted to crystallize from some basaltic andesites. In pseudoquaternary composition space, fractionating basaltic liquids will reach the pigeonite phase volume at either a reaction point (olivine + liquid → pigeonite + augite + plagioclase) or along a reaction curve (olivine + liquid → pigeonite) (Grove et al., 1983). The present study is an attempt to understand how cooling rate and volatile content affect the kinetics of this second peritectic reaction and how, for a basaltic andesite, the liquid line of descent varies as a function of cooling rate.

Our experimental results indicate that microphenocryst assemblages in the chilled margins of lava flows may not be the product of equilibrium crystallization and that internal differentiation of flows that are several meters in thickness may follow non-equilibrium paths (e.g., Kuno, 1965). We document four lava flows that exhibit the deviations predicted by our experiments. Finally, we suggest that these kinetic effects might be important during the flow of basaltic magma through dikes and conduits. Thermal models of magma flow in a dike predict that crystallization occurs at boundary layers under conditions of fairly rapid cooling, and metastable crystallization at such boundary layers might alter the compositions of the erupted lavas.

Experimental procedures

Starting material for all experiments was a powdered sample of Modoc basaltic andesite (Table 1) from the Callahan flow, Medicine Lake Highland, northern California (see Gerlach and Grove, 1982, for sample location of 79.38b). 30 to 40 mg of powder were sintered onto 0.1 mm diameter FePt alloy wire loops fabricated to be in equilibrium with the silicate charge (Grove, 1981). Samples were suspended in the hot spot of a Deltech DT31VT vertical quenching furnace. All experiments were run at the quartz-fayalite-magnetite buffer (QFM) using constant mixing propor-

0003–004X/85/0304–0279$02.00

Table 1. Composition of basaltic andesite 79.38b used in isothermal and cooling rate experiments

SiO_2	54.0
TiO_2	0.95
Al_2O_3	17.9
FeO	7.68
MnO	0.14
MgO	5.87
CaO	8.73
Na_2O	3.29
K_2O	0.97
Cr_2O_3	-
Sum	99.53

XRF analysis of 79.38b from J. Donnelly-Nolan, USGS (per. comm.)

tions of H_2–CO_2 or H_2–H_2O. In the latter case distilled water was boiled and a mixture of steam–H_2 was introduced into the top of the alumina muffle tube.

Oxygen fugacity was monitored using a CSIRO ZrO_2–CaO electrolyte cell (Arculus and Delano, 1981) calibrated at the Fe–FeO buffer. Temperature was monitored using Pt-Pt90/Rh10 thermocouples calibrated against the melting points of Au and Pd on the IPTS 1968 temperature scale (Biggar, 1972). All the samples were melted at 1170°C, 20°C below the liquidus, and contained plagioclase and olivine at the initiation of cooling. Samples were cooled at linear rates of 50°, 10°, 5°, 1°, and 0.5°C/hr. Each charge was cooled to a particular temperature and then quenched in water. Initial melt temperature and melt time were kept constant, as investigations of Lofgren and Smith (1980) and Lofgren (1983) show that these two variables may exert a control on the appearance temperature of a given phase. The initial melt temperature of 1170°C was chosen to provide a melt that was plagioclase + olivine-saturated at the beginning of cooling. Textural associations (Gerlach and Grove, 1982) suggest that 79.38b cooled from an initial temperature within the olivine + plagioclase stability field, and these experiments were designed to reproduce this crystallization history. Further, this experimental technique allowed us to investigate the effects of cooling rate and volatile content on pyroxene nucleation, because plagioclase and olivine are saturated at the initiation of cooling. Results are presented in Tables 2 and 3 and illustrated in Figures 1 through 3.

Infrared spectroscopic measurements (Stolper, 1982) were used to estimate the water contents of glasses run in the H_2–H_2O and H_2–CO_2 gas mixtures. Transmission spectra of the OH-stretching peak at 3550 cm^{-1} were obtained on the Perkin-Elmer model 180 spectrophotometer at Caltech, and the method discussed by Stolper (1982) was used to determine total water content. A sample run at 1200°C for 24 hours in the H_2–H_2O gas mixture (QFM) contained 0.095 wt.% total water, and a sample melted at 1210°C for 48 hours in H_2–CO_2 (QFM) contained 0.026 wt.% total water. At low total water contents hydroxyl groups are the dominant species of dissolved water in silicate melts, and under these conditions the square of the mole fraction of water in the melt, $(X^{melt}_{H_2O})^2$, is directly proportional to the fugacity of water in the gas phase, $(f^{gas}_{H_2O})$ (e.g., Russel, 1957; Uys and King, 1963). Using reaction constants from Deines et al. (1974) to calculate $f^{gas}_{H_2O}$ for the two gas mixtures, the results of our solubility experiments are consistent with the linear relationship between $f^{gas}_{H_2O}$ and $(X^{melt}_{H_2O})^2$. All the H_2–H_2O cooling rate experiments produced highly vesicular samples suggesting that water vapor was exsolving from the melt with decreasing temperature. Thus, ~0.1 wt.% H_2O must be considered a maximum value for water contents in samples run in the H_2–H_2O gas mixture. The H_2–CO_2 runs were not vesicular and probably have not exsolved a vapor phase.

Compositions of phases in the experimental runs were obtained with the M.I.T. 3-spectrometer MAC-5 electron microprobe using on-line data reduction and matrix correction procedures of Bence and Albee (1968) with modification of Albee and Ray (1970). A fused sample of USGS W-1 was used as a working standard and was analyzed before and after each experimental glass.

Experimental results

Equilibrium phase relations

Equilibrium appearance temperatures for plagioclase, olivine and pigeonite are shown in Figure 1; the data are from Grove et al. (1982) and from melting experiments reported in Table 2. Plagioclase is the liquidus phase (1192°C) followed by olivine (1172°C) and pigeonite (1140°C). The appearance temperature of plagioclase was identical within experimental error for both gas mixtures, and thus we assume that water contents $\leq$0.1 wt.% do not affect noticeably the equilibrium phase relations for this bulk composition.

Table 2. Results of melting and cooling rate experiments on 79.38b

Exp#	$T_{initial}$*	T_{final}	Duration hrs	Rate °C/hr	Gas mixture	Run products+
53	1200	1201	24.0	-	H_2-H_2O	gl+remnant plag
54	1183	1182	72.0	-	H_2-H_2O	gl+plag
108	1143	1146	229.2	-	H_2-CO_2	gl+plag+ol
119	1132	1133	166.7	-	H_2-H_2O	gl+plag+ol+pig
87	1171	1121	94.8	0.53	H_2-H_2O	gl+plag+ol
88	1171	1108	119.3	0.53	H_2-H_2O	gl+plag+ol+cpx
81	1170	1087	147.2	0.56	H_2-CO_2	gl+plag+ol
96	1171	1070	214.2	0.47	H_2-CO_2	gl+plag+ol+cpx
82	1170	1061	191.3	0.57	H_2-CO_2	gl+plag+ol+cpx
86	1170	1111	58.4	1.01	H_2-H_2O	gl+plag+ol
73	1170	1094	70.0	1.08	H_2-H_2O	gl+plag+ol+cpx
75	1169	1069	94.3	1.06	H_2-H_2O	gl+plag+ol+cpx
74	1170	1063	99.8	1.07	H_2-H_2O	gl+plag+ol+cpx
14	1170	1130	34.6	1.16	H_2-CO_2	gl+plag+ol
13	1169	1089	70.9	1.13	H_2-CO_2	gl+plag+ol
85	1171	1069	93.9	1.09	H_2-CO_2	gl+plag+ol+cpx
65	1170	1131	8.22	4.74	H_2-H_2O	gl+plag+ol
61	1170	1100	14.7	4.76	H_2-H_2O	gl+plag+ol
71	1170	1087	17.2	4.82	H_2-H_2O	gl+plag+ol
72	1170	1074	19.6	4.90	H_2-H_2O	gl+plag+ol
66	1171	1055	23.5	4.94	H_2-H_2O	gl+plag+ol+cpx
63	1170	1130	8.50	4.70	H_2-CO_2	gl+plag+ol
57	1170	1099	14.6	4.86	H_2-CO_2	gl+plag+ol
67	1171	1082	19.6	4.54	H_2-CO_2	gl+plag+ol
64	1170	1056	24.2	4.71	H_2-CO_2	gl+plag+ol+cpx
99	1171	1060	11.3	9.81	H_2-H_2O	gl+plag+ol
100	1171	1050	12.3	9.80	H_2-H_2O	gl+plag+ol+cpx
83	1171	1065	11.1	9.55	H_2-CO_2	gl+plag+ol
84	1171	1052	12.3	9.67	H_2-CO_2	gl+plag+ol+cpx
120	1170	1039	2.75	47.6	H_2-H_2O	gl+plag+ol
104	1171	1008	3.47	47.0	H_2-H_2O	gl+plag+ol+cpx
109	1170	1035	2.82	47.4	H_2-CO_2	gl+plag+ol
110	1170	1014	3.28	47.6	H_2-CO_2	gl+plag+ol+cpx

*Experiments were held at T_{init} for 24 hrs, then cooled at the specified rate and quenched into water at T_{fin}; #13 was melted for 23.25 hours.

+The abbreviations used are: gl = quenched liquid, plag = plagioclase, ol = olivine, pig = pigeonite, cpx = clinopyroxene, either augite or pigeonite. Charges contain plagioclase and minor olivine at the initiation of cooling.

Table 3. Electron microprobe analyses of run products from cooling rate experiments

Run#	Phase	# of analyses	SiO_2	TiO_2	Al_2O_3	FeO	MnO	MgO	CaO	Na_2O	K_2O	Cr_2O_3	Total
66	gl	5	59.8(6)*	2.09(6)	11.6(1)	9.48(50)	0.26(3)	3.42(16)	8.07(28)	2.60(6)	1.69(12)	0.02(2)	99.03
64	gl	4	60.0(7)	2.06(6)	11.9(9)	10.4(2)	0.24(2)	3.39(13)	7.94(17)	2.66(5)	1.76(7)	0.02(2)	100.37
85	gl	9	60.9(6)	1.88(7)	12.5(4)	9.81(43)	0.17(2)	2.98(19)	7.27(33)	3.07(34)	1.85(6)	0.02(2)	100.42
	cpx†		50.8	1.34	2.78	9.85	0.23	13.9	19.9			0.11	98.96
	cpx		51.2	1.32	3.29	10.2	0.30	14.8	18.8			0.11	100.04
	ol		35.7	0.03	0.23	30.5	0.47	31.1	0.34			0.09	98.57
73	gl	8	60.7(9)	1.76(8)	13.3(1)	7.36(46)	0.20(4)	3.96(16)	7.92(23)	3.07(29)	1.60(6)	0.03(2)	99.87
	cpx		52.3	0.92	2.16	7.11	0.35	17.0	19.8			0.19	99.85
	cpx		52.4	0.92	2.34	8.00	0.33	18.4	17.4			0.42	100.12
	ol		38.8	0.05	0.27	21.5	0.47	39.8	0.45			0.10	101.44
74	gl	7	64.7(3)	2.21(14)	13.1(2)	6.90(36)	0.17(4)	2.07(8)	5.12(21)	2.10(23)	2.27(10)	0.01(1)	98.65
	cpx		50.9	1.64	3.20	7.85	0.35	15.7	19.7			0.13	99.44
	cpx		51.4	1.31	2.42	9.98	0.45	17.7	16.8			0.10	100.09
	ol		37.2	0.09	0.42	26.8	0.61	32.5	0.82			0.02	98.91
88	gl	8	59.8(6)	1.67(6)	13.5(2)	7.27(16)	0.18(2)	4.40(8)	8.00(18)	2.74(16)	1.46(4)	0.02(2)	99.04
	cpx		52.4	0.97	2.49	7.30	0.33	19.2	17.5			0.35	100.54
	cpx		53.0	0.74	1.95	7.75	0.39	21.6	13.9			0.28	99.53
	cpx		54.7	0.42	2.45	10.0	0.39	27.1	6.26			0.26	101.63
	ol		38.6	0.04	0.34	19.1	0.47	40.9	0.40			0.04	99.92
96	gl	6	60.4(4)	2.03(9)	12.7(1)	9.92(34)	0.19(4)	2.59(15)	6.24(23)	3.39(14)	1.82(3)	0.02(2)	99.27
	cpx		51.3	1.14	2.65	9.65	0.26	14.8	19.7			0.20	99.70
	cpx		51.4	1.12	2.08	12.8	0.38	16.2	14.2			0.13	98.31
	ol		35.7	0.09	0.35	33.1	0.61	29.7	0.54			6.07	100.16
82	gl	6	62.2(5)	2.31(11)	12.6(1)	9.41(33)	0.16(2)	2.12(15)	5.23(13)	2.22(10)	2.28(8)	0.00	98.53
	cpx		51.1	1.07	2.58	9.32	0.26	15.1	20.5			0.33	100.19
	cpx		51.2	1.10	1.96	13.3	0.30	15.3	17.2			0.06	100.45
	cpx		52.0	0.70	1.30	19.6	0.50	19.8	5.35			0.09	99.38
	ol		35.7	0.04	0.12	34.6	0.60	28.5	0.38			0.02	99.97

*Parenthesized units represent one standard deviation of replicate analyses in terms of least units cited, i.e. 59.8(6) = 59.8±0.6.

†Abbreviations as in Table 2; clinopyroxene and olivine compositions represent single analyses; reported clinopyroxene data span the range of observed Wo contents; olivine analyses are representative of observed rim compositions.

Non-equilibrium phase relations

Pyroxene appearance temperatures. Figure 1 also summarizes the pyroxene appearance temperature vs. cooling rate data and shows graphically how cooling rate and the amount of dissolved H_2O affect the kinetics of clinopyroxene nucleation in 79.38b. Run times, quench temperatures and phases present are recorded in Table 2. Experiments below the two "pyroxene in" lines in Figure 1 contain clinopyroxene (cpx) in the charge, and Figure 1 shows that clinopyroxene nucleation is increasingly supercooled with respect to its equilibrium temperature as cooling rates increase from 0.5°C/hr to 50°C/hr. In the 50° and 10°C/hr experiments carried out in both H_2–H_2O and H_2–CO_2 gas mixtures, clinopyroxene appearance temperatures are indistinguishable, and augite crystallization is supercooled by 115° and 85°C respectively. At 5°C/hr the appearance temperatures of augite for the two gas mixtures are identical within the experimental constraints, and $\Delta T = 70°$ to 75°C (ΔT = difference between isothermal appearance temperature and cooling rate appearance temperature). At a cooling rate of 1°C/hr augite crystallizes at ~1077°C and is supercooled by 60–65°C in the H_2–CO_2 gas mixture. At the same cooling rate but in the H_2–H_2O mixture the appearance temperature and degree of supercooling are 1100°C and ~40°C respectively. At the slowest cooling rate studied, 0.5°C/hr, the ΔT's are 55° to 60°C (H_2–CO_2) and 25°C (H_2–H_2O).

Pyroxene chemistry variations. Figures 2a and b summarize the compositions of the first pyroxenes to crystallize in the H_2–H_2O and H_2–CO_2 1°C/hr and 0.5°C/hr cooling rate experiments; selected compositions are reported in Table 3. Pyroxene grains in the more rapidly cooled runs were too small for quantitative analysis by electron microprobe, but in all cases qualitative analysis showed them to be Ca,Al-rich augites. The first pyroxene to crystallize in the 1° and 0.5°C/hr H_2–CO_2 experiments is augite. Augite is also the sole pyroxene in the H_2–H_2O 1°C/hr experiment, while the 0.5°C/hr run contains augite and pigeonite that appear to have nucleated simultaneously. Note that early crystallization of augite is inconsistent with the equilibrium phase relations presented in Figure 1. Under equilibrium conditions the first pyroxene to crystallize from 79.38b is pigeonite. Figure 2 also shows that at the same

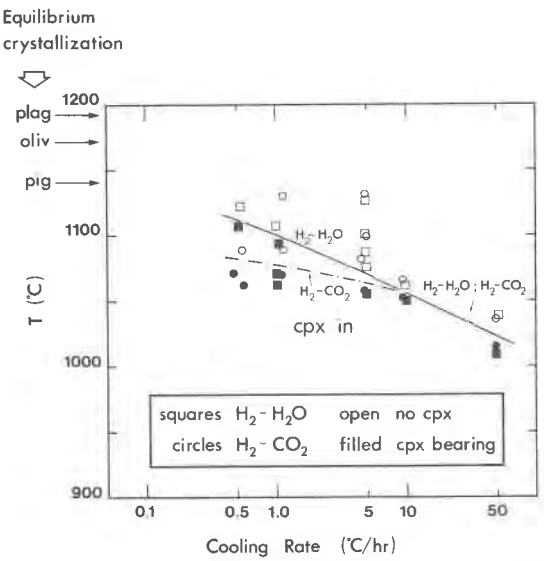

Fig. 1. Pyroxene appearance temperature as a function of cooling rate and gas mixture. Each experiment was initiated at 1170°C, cooled at a particular rate and quenched at the temperature indicated by the symbol. Near-liquidus equilibrium phase relations are shown in the upper left-hand corner.

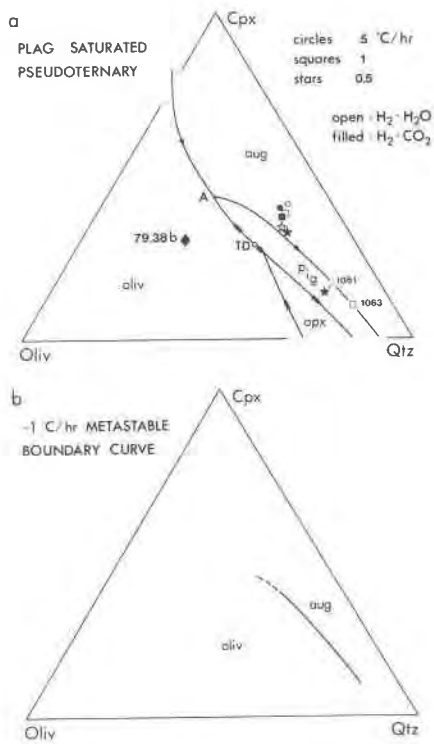

Fig. 3. (a) Compositions of pyroxene-saturated liquids from the 5, 1, and 0.5°C/hr experiments projected onto the olivine (Oliv)–clinopyroxene (Cpx)–silica (Qtz) pseudoternary of Grove et al. (1982). Additional abbreviations are aug = augite, pig = pigeonite, opx = orthopyroxene and TD = thermal divide. The projection uses oxygen units, see Grove et al. (1982, 1983) for the necessary algorithms. The diamond represents the projected position of the bulk composition used in this study; open and closed symbols denote the H_2–H_2O and H_2–CO_2 experiments, respectively. The plagioclase-saturated equilibrium phase relations are from Walker et al. (1979), Grove et al. (1982, 1983) and Grove and Bryan (1983). (b) Projected position of the metastable oliv–aug–plag cotectic based on the 1°C/hr experimental liquids in Fig. 3a. Compared to the equilibrium phase relations the olivine field has expanded, the pigeonite field has disappeared and the augite field has contracted.

cooling rate the initial pyroxenes in the H_2–H_2O experiments are more Mg-rich than those in the H_2–CO_2 runs and generally exhibit greater variations in Wo content at relatively constant Mg*-values (where Mg* = Mg/[Mg + Fe_{total}], atomic). With decreasing cooling rate augites in both the H_2–H_2O and H_2–CO_2 experiments trend toward lower Ca contents. For example, in the 1°C/hr run quenched at 1094°C the augite compositions form a band from $Wo_{41}En_{45}$ to $Wo_{34}En_{50}$, while in the 0.5°C/hr run with T_{quench} = 1108°C the spectrum is Wo_{35-27} En_{54-60}. Pigeonites in this 0.5°C/hr run are high in Ca with Wo values in the range 12 to 16.

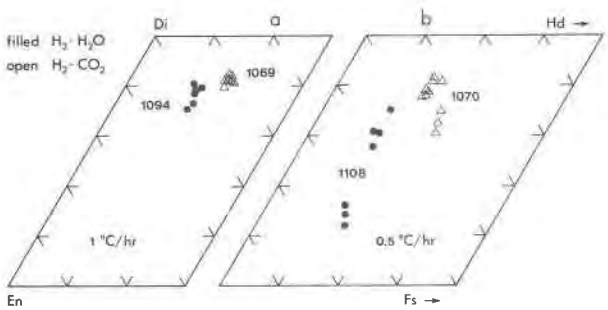

Fig. 2. Pyroxene compositional variations observed in the H_2–H_2O and H_2–CO_2 controlled cooling rate experiments that are first saturated with clinopyroxene. Number by each group of symbols is the quench temperature of that experiment. (a) Pyroxenes in the 1°C/hr runs. (b) Pyroxenes in the 0.5°C/hr runs.

Discussion

Nucleation and crystallization processes

The increase in the appearance temperature of a phase with decreasing cooling rate has been noted in anhydrous CO–CO_2 experiments on lunar basalts (Walker et al., 1976; Grove and Bence, 1977; Grove, 1978; Gamble and Taylor, 1980) and on a basaltic achondrite (Walker et al., 1978) and has been inferred from petrographic studies of tholeiitic pillow basalts (Bryan, 1972; Kirkpatrick, 1978). In general, an increase in appearance temperature associated with a decrease in cooling rate reflects the higher probability of nucleation occurring near the equilibrium temper-

ature at very slow cooling rates. For the basaltic andesite studied here approximately 0.1 wt.% H_2O dissolved in the melt partially offsets cooling rate induced phase suppression at rates <5°C/hr. The effect of water can be rationalized by considering its ability to depolymerize silicate melts and is consistent with recent kinetic theories of nucleation (Kirkpatrick, 1983). The main feature of Kirkpatrick's model is that the addition of individual tetrahedra from the melt to a proto-nucleus is the rate controlling step in nucleation, and that the activation energy of this process is proportional to the number of tetrahedral cation–oxygen bonds that are broken in reducing the polymer units in the melt to single tetrahedra, and the number of bonds that are broken in attaching these individual tetrahedra to a proto-nucleus. Since the number of tetrahedral cation–oxygen bonds that have to be broken to attach a tetrahedron to a given clinopyroxene nucleus will be the same under anhydrous or hydrous conditions, only the degree of polymerization in the melt affects the total activation energy. If dissolved water increases the number of SiO_4^{-4} units in the melt, the probability that nucleation will occur at a given degree of undercooling will also increase, and one would expect this ΔT to be smaller than that required for nucleation in a more polymerized anhydrous melt. This rationale is consistent with the results of the <5°C/hr cooling rate experiments. At cooling rates greater than 5°C/hr augite crystallization occurs at approximately the same temperatures in the H_2–H_2O and H_2–CO_2 experiments. This behavior is controlled by the exponential decrease in diffusion rates in the melt with decreasing temperature. At slow cooling rates a large time interval is spent at high temperatures, and the diffusion of melt species to a proto-nucleus is not a rate-limiting step in the nucleation and growth process. However, at rapid cooling rates the time spent at high temperatures is short, and with decreasing temperature diffusion rate slows and becomes the rate-controlling mechanism.

Variations in Wo content in "rapidly" cooled clinopyroxenes have been noted by Smith and Lindsley (1971) in samples from the base of a Columbia River basalt flow, by Evans and Moore (1968) in quenched samples from the tholeiitic Makaopuhi Lava Lake, Hawaii, and by Nakamura and Coombs (1973) in outer sections of a doleritic intrusion in New Zealand. Smith and Lindsley (1971) concluded that such trends represent metastable pyroxene-liquid partitioning caused by rapid crystallization. Similar trends have been produced in cooling rate experiments (from 0.5° to >100°C/hr) on lunar basalts (Grove and Bence, 1979; Gamble and Taylor, 1980) and on a Columbia River Grande Ronde basalt (Schiffman and Lofgren, 1982). In all of these cases pyroxene crystallization progressed over an appreciable temperature interval and it is difficult to separate the effects of changes in liquid composition (a depletion in Ca as crystallization proceeds) from those caused by metastable fluctuations in the Ca distribution coefficient (K_d) for augite–liquid. Similar trends are seen in the Wo contents of clinopyroxenes produced in this study (Fig. 2a, b), and the small modal abundance of augite in the 0.5°C/hr experiments quenched at 1108°C implies that the liquid composition remained nearly constant during pyroxene crystallization. Thus, the variations in Wo component in the clinopyroxenes in the 0.5°C/hr experiment reflect either rate dependent changes in K_d^{CaO} or the presence of disequilibrium high- and low-Ca pyroxene domains in each crystal that are smaller than the microprobe beam.

Equilibrium and non-equilibrium liquid lines of descent

Equilibrium and metastable crystallization paths followed by liquids of bulk composition 79.38b can be compared graphically using a projection scheme and phase diagram presented in Grove et al. (1982, 1983) (Fig. 3a). All cotectics and reaction curves on this olivine (Oliv)–clinopyroxene (Cpx)–silica (Qtz) pseudoternary are saturated with plagioclase (Plag) in addition to the two phases noted on either side of each boundary curve. Under equilibrium conditions a liquid of composition 79.38b crystallizes plagioclase and olivine as liquidus phases, and the projected residual liquid moves away from the olivine corner until it reaches the oliv–pigeonite (pig)–plag reaction curve where olivine is resorbed and pigeonite crystallizes (Fig. 3a). Note that the crystallization sequence predicted from the Oliv–Cpx–Qtz pseudoternary is consistent with the experimentally determined phase relations, which are plagioclase and olivine crystallization followed by pigeonite crystallization.

Figure 3a also shows the projected residual liquid compositions from the H_2–H_2O and H_2–CO_2 5°, 1° and 0.5°C/hr cooling rate experiments that mark the first appearance of clinopyroxene. Both pairs of 5° and 1°C/hr experiments and the H_2–CO_2 0.5°C/hr run contain only augite (<5%), and the residual liquids from these experiments project onto the augite (aug)–plag phase volume. Under these cooling rate conditions the residual liquids traversed the pig–plag phase volume on approximate trajectories away from the olivine corner. The apparent curvature is due to the loss of Na during the course of the experiments, which moves projected liquid compositions toward the quartz apex of the pseudoternary. Calculated Fe-Mg exchange coefficients (K_D^{Fe-Mg}) for augite–liquid pairs fall in the range 0.21 to 0.26 (where $K_D^{Fe-Mg} = X_{Fe}^{xtal} X_{Mg}^{liq} / X_{Mg}^{xtal} X_{Fe}^{liq}$; total Fe as Fe^{2+}). These values overlap the augite K_D^{Fe-Mg} values determined in isothermal melting experiments on calc-alkaline series volcanics (Grove et al., 1982) and mid-ocean ridge basalts (Grove and Bryan, 1983). Olivine is a crystallizing phase in all five experiments, and rim compositions of abundant <50 μm-sized euhedral olivine crystals yield K_D^{Fe-Mg} values of 0.27 to 0.30. Augite and pigeonite appear to have crystallized simultaneously in the H_2–H_2O 0.5°C/hr experiment, and significantly the projected liquid composition falls very close to the equilibrium pig–aug–plag cotectic. Augite and pigeonite K_D^{Fe-Mg} values are both 0.24. Liquid compositions from two experiments that have crystallized pyroxene over a 20° to 30°C temperature interval are also projected in Figure

3a, and give an indication of the liquid path followed with further cooling. As expected, both of these compositions have higher SiO_2 contents and lower Mg/Fe ratios than the higher temperature pyroxene-saturated liquids. The liquid in the 1°C/hr H_2–H_2O run quenched at 1063°C coexists with augite, olivine and plagioclase, while the 0.5°C/hr H_2–CO_2 experiment quenched at 1061°C contains augite, olivine, plagioclase and minor pigeonite. Taken together, the experimental liquids can be used to construct an idealized metastable phase diagram appropriate for 79.38b and cooling rates of ~1°C/hr (Fig. 3b). Note that the equilibrium pig–aug–plag cotectic has been replaced by a metastable oliv–aug–plag boundary curve. Compared to the equilibrium phase relations (Fig. 3a) the olivine field has expanded, the pigeonite field has disappeared and the oliv–aug–plag cotectic extends metastably to more quartz normative compositions.

The replacement of equilibrium pigeonite as the initial pyroxene by augite or augite + pigeonite during dynamic crystallization is clearly demonstrated in this study and has been observed for a number of lunar bulk compositions (Walker et al., 1976; Grove, 1978) and for a Columbia River basalt (Schiffman and Lofgren, 1982). Figure 3a shows that if pigeonite nucleation is suppressed, bulk composition 79.38b continues to crystallize olivine and plagioclase, and the residual liquid moves through the pig–plag phase volume and into the aug–plag phase volume. When pyroxene nucleates the residual liquid has entered the augite phase volume and crystallizes augite. This relationship is shown schematically in Figure 4, which represents an idealized temperature-composition pseudoliquidus section through the pig–plag phase volume radial to the olivine corner of the Oliv–Cpx–Qtz pseudoternary (Fig. 3a). If pigeonite appearance is suppressed, the metastable oliv–plag surface reaches the aug–plag surface and generates a metastable oliv–aug–plag cotectic. Dissolved H_2O allows pigeonite to crystallize by decreasing the extent to which the pyroxene appearance temperature is suppressed, so that residual liquids have not moved through the pigeonite volume before pyroxene nucleates.

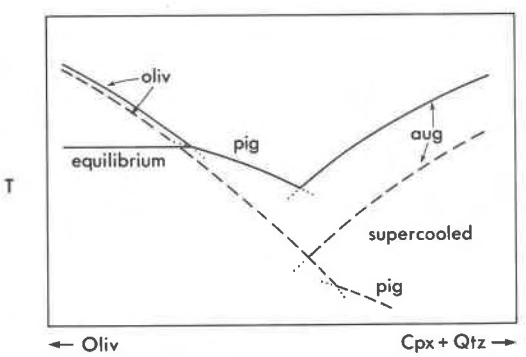

Fig. 4. Schematic pseudoliquidus section through the oliv–pig–plag reaction curve and the pig–aug–plag cotectic (Fig. 3a). Solid lines represent equilibrium configuration of the pseudoliquidus surfaces; dashed lines represent supercooled conditions where pigeonite has been suppressed to a greater extent than augite. The metastable extension of the oliv–plag surface reaches the aug–plag surface and creates a metastable oliv–aug–plag cotectic.

Calculated thermal histories

The kinetic effects described above occur over the range of cooling rates that are experienced by basaltic liquids cooling in dikes and sills or cooling near the upper surfaces of lava flows and lava lakes. The thermal histories of flows and sills can be approximated by analytical heat flow solutions that include the effects of latent heat of solidification. We have used conductive cooling models to calculate cooling rates as a function of distance from the boundary of heat loss. Jaeger provides solutions for the case of a dike (Jaeger, 1957, equation 10) and for the upper surface of a lava flow (Jaeger, 1968, equation 36). These analytical solutions can then be used to approximate cooling rates using the method of Jaeger (1957), who expanded the treatment of Winkler (1949). The calculations have been performed for our basaltic lava assuming liquidus and solidus temperatures of 1200° and 1000°C, respectively, a value for the latent heat of 80 cal/gm and thermal conductivity and diffusivity values of 0.005 cal/sec cm°C and 0.0052 cm^2/sec. Cooling rates were calculated over the temperature interval 1150° to 1100°C. For the case of cooling within a dike or sill-like body, cooling rates of 1.0°, 0.5°, 0.1°, and 0.05°C/hr are estimated to occur at the centers of dikes with half thicknesses of 1.0, 1.3, 3.0 and 4.2 m. In the case of solidification at the upper free surface of a lava flow, cooling rates of 1.0°, 0.5°, 0.1°, and 0.05°C/hr are predicted to occur within layers that are 1.7, 2.5, 5.5 and 7.8 m below the flow surface. Although the effects of hydrothermal circulation, differentiation and convection are neglected in these calculations, the results are generally correct to an order of magnitude. Jaeger (1968) provides a comprehensive review of the limitations of these calculations, and Huppert et al. (1984) discuss the effects of convection and show that the conductive assumption holds for lavas with physical properties of basalts and basaltic andesites.

It may be concluded that pigeonite suppression and metastable crystallization of olivine, augite and plagioclase are expected to occur near the margins of small magma bodies. The considerations discussed above suggest that the kinetic effects may be important during cooling of magmas within 3 meters of the heat loss boundary of a dike and within 5 m of the upper surface of a lava flow. In the next section we will show that field evidence supports the results of these calculations.

Field observations

Field associations and textural and compositional information in basaltic lava flows further support the operation of these kinetic processes in the thermal environments experienced by cooling lava flows. Segregation veins are common in many lava flows (e.g., Kuno, 1965; Smith, 1967; Sato, 1978), and the textural and compositional characteristics of these veins can be used to infer the liquid line of descent followed during within-flow solidification.

Figure 5 shows the projected compositions of matrix and adjacent glassy segregation veins from three Medicine Lake basaltic andesite (BA) lava flows (Anderson et al., 1984). The samples were located 1 to 2.5 m from either the tops or bottoms of their respective flows. The crystal matrix found in association with the segregated melt is plagioclase, olivine, augite and magnetite. The phase assemblage and glass compositions are those that would be predicted from the results of our slow cooling rate experiments (1° and 0.5°C/hr) and are consistent with the cooling rates estimated for the portions of the lava flows in which the segregation veins are found. If these portions of the flows had crystallized under equilibrium conditions, one would predict pigeonite to be a saturating phase, since plagioclase + olivine crystallization in all three natural compositions (Fig. 5) will drive residual liquids toward the oliv–pig–plag reaction curve. Apparently pigeonite did not crystallize during cooling, and residual liquids moved through the pig–plag phase volume and nucleated augite. Further crystallization involved plagioclase, olivine, augite and magnetite. The bulk compositions of the lavas discussed by Anderson et al. (1984) plot within the olivine primary phase volume and have followed a metastable liquid line of descent that is topologically similar to the metastable cotectic determined by the cooling rate experiments (Fig. 3b).

If pigeonite nucleation is also suppressed for bulk compositions that project above the line connecting Oliv and point A, residual liquids moving down the oliv–aug–plag cotectic might pass through reaction point A and proceed down a metastable extension of the oliv–aug–plag boundary curve. Such liquids would not undergo the reaction relation that occurs at point A (Fig. 3a). Since most basaltic compositions reach the oliv–aug–plag cotectic during low-pressure crystallization and proceed to reaction point A, metastable crystallization of olivine, augite and plagioclase may explain the absence of groundmass pigeonite in some basalts. For example, Figure 6 shows pyroxene and olivine compositions in a high alumina basalt (HAB) from Giant Crater, Medicine Lake Highland. The sample was located in a filled lava tube approximately 41 cm from a vertical conductive heat loss boundary and has an intergranular to subophitic texture. Clinopyroxenes range from granular (<50 μm) to radiating acicular laths and are zoned from $Wo_{45}En_{45}$ to $Wo_{43}En_{11}$. Microphenocryst and groundmass olivines range from Fo_{88} to Fo_{33}. Experimentally determined olivine, pigeonite and augite compositions that coexist with liquid at reaction point A are also shown for this same HAB (Grove et al., 1982). The sample from 41 cm was chosen as an example because of the dramatic compositional zoning that developed in the olivine and augite. The Giant Crater lava tube fill has a half width of 6 m, and pigeonite has not been found anywhere in the cooling unit.

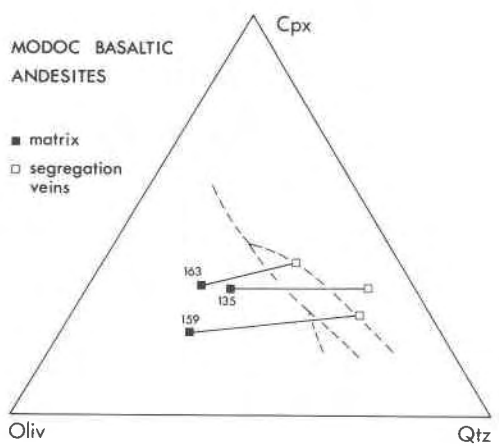

Fig. 5. Coexisting crystalline matrix and glassy segregation veins from three Modoc basaltic andesite flows, Medicine Lake, northern California, projected onto the Oliv–Cpx–Qtz pseudoternary. Numbers by the solid squares refer to sample designations in Table 3 of Anderson et al. (1984). The solid lines connect related matrix and segregation vein pairs. Plagioclase saturated equilibrium phase relations (dashed lines) are shown for reference.

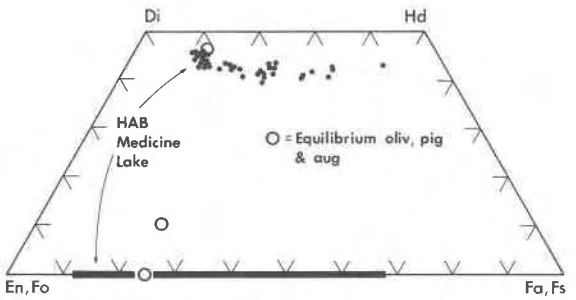

Fig. 6. Coexisting groundmass augites and olivines in a high alumina basalt (HAB) from Giant Crater, Medicine Lake. Open circles represent experimental olivine, pigeonite and augite compositions in equilibrium with liquid at reaction point A (Fig. 3a) for this same HAB (Grove et al., 1982).

The Giant Crater HAB projects above the line Oliv-A in the pseudoternary system (Fig. 3a) and crystallizes olivine and plagioclase as liquidus phases (Grove et al., 1982). When augite joins the crystallizing assemblage, residual liquid moves down the oliv–aug–plag cotectic to reaction point A. Under conditions of either equilibrium or fractional crystallization, pigeonite crystallizes and residual liquids either solidify completely at A or move down the aug–pig–plag cotectic. In either case the most Fe-rich olivine that should crystallize from the HAB is Fo 75-70. However, under the cooling conditions experienced by the Giant Crater HAB sample pigeonite failed to nucleate. The Fe-rich olivine present in this rock (Fig. 6) indicates that liquids moved through point A and continued along a metastable oliv–aug–plag cotectic.

Richardson (1979) describes an 80 to 110 m thick Karroo diabase sheet that consists of a chilled zone within 5 cm of the lower contact and a coarse-grained diabase interior. The chilled margin is composed of plagioclase, olivine and augite microphenocrysts set in a microcrystalline groundmass of plagioclase, augite and opaques. The bulk of the sill consists of subophitic intergrowths of

pyroxene and plagioclase enclosing anhedral grains of olivine. Although augite and pigeonite are the dominant mafic phases in the interior of the sill, pigeonite is absent in the region between 3 and 4 m above the basal contact. Although bulk composition must in part control the extent to which pigeonite nucleation can be suppressed, the calculated cooling rates for the first appearance of pigeonite in the sill (0.1 to 0.05°C/hr) are slower than the rates inferred for the two examples above where pigeonite is absent.

Kinetic effects such as non-equilibrium crystallization may be important during the ascent of basaltic magma in dikes through the upper crust. Delaney and Pollard (1982) have modeled the heat transfer that occurs during magma flow through a dike, incorporating field observations of flow rates of basaltic eruptions and measurements of average dike widths exposed in Iceland, Scotland and the Colorado Plateau. One result of their analysis is that magmas flowing through dikes in the upper crust over distances of more than a few kilometers and at rates typical of basaltic eruptions will solidify within 10's to 100's of hours. One would expect the kinetic effects discussed here to be important in the solidification of these dikes and the phase assemblages and residual liquids to depart from equilibrium in the manner modeled by our rate experiments. Such dikes are common geological phenomena, and disequilibrium effects may play an important role in their solidification.

The analysis of Delaney and Pollard (1982) also predicts the development of an advancing solidification front-thermal boundary layer that grows into the fluid center of the dike. The thermal evolution of this boundary can be calculated for dike widths and flow rates that are typical of those observed in plutonic and volcanic basaltic provinces. The results show that cooling rates in the advancing solidification front of a 2 m thick dike are on the order of 1°C/hr. If a kinetically-influenced crystal assemblage grows at this advancing interface and the remaining liquid is removed by flow through the conduit, such a process could influence the compositions of the volcanic products. One might find such compositional variations to be well developed during the initial "curtain of fire" eruptive stage of a volcanic system and to be diminished in later eruptive episodes where a central vent supplied magma to the surface. Thus, kinetic effects may influence the compositions of residual liquids generated by fractional crystallization in extrusive rocks or rocks from small intrusive bodies.

Acknowledgments

This research was supported by NSF grant EAR-8200373. The authors thank Julie Donnelly-Nolan for supplying major element data and Ed Stolper for access to, and assistance with, the infrared spectrophotometer. We thank Stan Hart, Dean Presnall and Dave Walker for critical reviews.

References

Albee, A. L. and Ray, Lily (1970) Correction factors for electron probe microanalysis of silicates, oxides, carbonates, phosphates and sulfates. Analytical Chemistry, 42, 1408–1414.

Anderson, A. T., Jr., Swihart, G. H., Artioli, Gilberto, and Geiger, C. A. (1984) Segregation vesicles, gas filter-pressing, and igneous differentiation. Journal of Geology, 92, 55–72.

Arculus, R. J. and Delano, J. W. (1981) Intrinsic oxygen fugacity measurements: techniques and results for spinels from upper mantle peridotites and megacryst assemblages. Geochimica et Cosmochimica Acta, 45, 899–914.

Bence, A. E. and Albee, A. L. (1968) Empirical correction factors for the electron microanalysis of silicates and oxides. Journal of Geology, 76, 382–403.

Bianco, A. S. and Taylor, L. A. (1977) Applications of dynamic crystallization studies: Lunar olivine-normative basalt. Proceedings of the 8th Lunar Science Conference, 1593–1610.

Biggar, G. M. (1972) Diopside, lithium metasilicate, and the 1968 temperature scale. Mineralogical Magazine, 38, 768–770.

Bryan, W. B. (1972) Morphology of quench crystals in submarine basalts. Journal of Geophysical Research, 77, 5812–5819.

Deines, Peter, Nafziger, R. H., Ulmer, G. C., and Woermann, Edward (1974) Temperature–oxygen fugacity tables for selected gas mixtures in the system C–H–O at one atmosphere total pressure. Bulletin of Earth and Mineral Sciences Experimental Station, 88, 129 p.

Delaney, P. T. and Pollard, D. D. (1982) Solidification of basaltic magma during flow in a dike. American Journal of Science, 282, 856–885.

Evans, B. W. and Moore, J. G. (1968) Mineralogy as a function of depth in the prehistoric Makaopuhi tholeiitic lava lake, Hawaii. Contributions to Mineralogy and Petrology, 17, 85–115.

Gamble, R. P. and Taylor, L. A. (1980) Crystal/liquid partitioning in augite: Effects of cooling rate. Earth and Planetary Science Letters, 47, 21–33.

Gerlach, D. C. and Grove, T. L. (1982) Petrology of Medicine Lake Highland volcanics: Characterization of endmembers of magma mixing. Contributions to Mineralogy and Petrology, 80, 147–159.

Grove, T. L. (1978) Cooling histories of Luna 24 very low Ti (VLT) ferrobasalts: An experimental study. Proceedings of the 9th Lunar and Planetary Science Conference, 565–584.

Grove, T. L. (1981) Use of FePt alloys to eliminate the iron loss problem in 1-atmosphere gas mixing experiments: Theoretical and practical considerations. Contributions to Mineralogy and Petrology, 78, 298–304.

Grove, T. L. and Bence, A. E. (1977) Experimental study of pyroxene–liquid interaction in quartz-normative basalt 15597. Proceedings of the 8th Lunar Science Conference, 1549–1579.

Grove, T. L. and Bence, A. E. (1979) Crystallization kinetics in a multiply saturated basalt magma: An experimental study of Luna 24 ferrobasalt. Proceedings of the 10th Lunar and Planetary Science Conference, 439–478.

Grove, T. L. and Bryan, W. B. (1983) Fractionation of pyroxene-phyric MORB at low pressure: An experimental study. Contributions to Mineralogy and Petrology, 84, 293–309.

Grove, T. L. and Raudsepp, Mati (1978) Effects of kinetics on the crystallization of quartz normative basalt 15597: An experimental study. Proceedings of the 9th Lunar and Planetary Science Conference, 585–599.

Grove, T. L., Gerlach, D. C., and Sando, T. W. (1982) Origin of calc-alkaline series lavas at Medicine Lake Volcano by fractionation, assimilation and mixing. Contributions to Mineralogy and Petrology, 80, 160–182.

Grove, T. L., Gerlach, D. C., Sando, T. W., and Baker, M. B. (1983) Origin of calc-alkaline series lavas of Medicine Lake volcano by fractionation, assimilation and mixing: corrections and

clarifications. Contributions to Mineralogy and Petrology, 82, 407–408.

Huppert, H. E., Sparks, R. S. J., Turner, J. S., and Arndt, N. T. (1984) Emplacement and cooling of komatiite lavas. Nature, 309, 19–22.

Jaeger, J. C. (1957) The temperature in the neighborhood of a cooling intrusive sheet. American Journal of Science, 255, 306–318.

Jaeger, J. C. (1968) Cooling and solidification of igneous rocks. In H. H. Hess and Arie Poldervaart, Eds., Basalts, The Poldervaart Treatise on Rocks of Basaltic Composition, vol. 2, p. 503–536. Wiley-Interscience, New York.

Kirkpatrick, R. J. (1978) Processes of crystallization in pillow basalts, hole 396B, DSDP Leg 46. In Leonid Dmitriev, James Heirtzler, et al., Eds., Initial Reports of the Deep Sea Drilling Project, vol. 46, p. 271–282. U.S. Government Printing Office, Washington, D.C.

Kirkpatrick, R. J. (1983) Theory of nucleation in silicate melts. American Mineralogist, 68, 66–77.

Kirkpatrick, R. J., Reck, B. H., Pelly, I. Z., and Kuo, Lung-Chuan (1983) Programmed cooling experiments in the system MgO–SiO_2: kinetics of a peritectic reaction. American Mineralogist, 68, 1095–1101.

Kuno, Hisashi (1965) Fractionation trends of basalt magmas in lava flows. Journal of Petrology, 6, 302–321.

Lofgren, G. E. (1983) Effect of heterogeneous nucleation on basaltic textures: A dynamic crystallization study. Journal of Petrology, 24, 229–255.

Lofgren, G. E. and Smith, D. P. (1980) The experimental determination of cooling rates of rocks: Some complications. Lunar and Planetary Science XI, 631–633. Lunar and Planetary Institute, Houston.

Lofgren, G. E., Donaldson, C. H., Williams, R. J., Mullins, Oscar, and Usselman, T. M. (1974) Experimentally reproduced textures and mineral chemistry of Apollo 15 quartz normative basalts. Proceedings of the 5th Lunar Science Conference, 549–568.

Nakamura, Y. and Coombs, D. S. (1973) Clinopyroxenes in the Tawhiroko tholeiitic dolerite at Moeraki, north-eastern Otago, New Zealand. Contributions to Mineralogy and Petrology, 42, 213–228.

Richardson, S. H. (1979) Chemical variation induced by flow differentiation in an extensive Karroo dolerite sheet, southern Namibia. Geochimica et Cosmochimica Acta, 43, 1433–1441.

Russell, L. E. (1957) Solubility of water in molten glass. Journal of the Society of Glass Technology, 41, 304–317T.

Sato, Hiroaki (1978) Segregation vesicles and immiscible liquid droplets in ocean-floor basalt of Hole 396B, IPOD/DSDP Leg 46. In Leonid Dmitriev, James Heirtzler et al., Eds., Initial Reports of the Deep Sea Drilling Project, vol. 46, p. 283–291. U.S. Government Printing Office, Washington, D.C.

Schiffman, Peter and Lofgren, G. E. (1982) Dynamic crystallization studies on the Grande Ronde pillow basalts, central Washington. Journal of Geology, 90, 49–78.

Smith, Douglas and Lindsley, D. H. (1971) Stable and metastable augite crystallization trends in a single basalt flow. American Mineralogist, 56, 225–233.

Smith, R. E. (1967) Segregation vesicles in basaltic lava. American Journal of Science, 265, 696–713.

Stolper, Edward (1982) Water in silicate glasses: An infrared spectroscopic study. Contributions to Mineralogy and Petrology, 81, 1–17.

Uys, J. M. and King, T. B. (1963) The effect of basicity on the solubility of water in silicate melts. Transactions of the Metallurgical Society of A.I.M.E., 227, 492–500.

Walker, David, Shibata, Tsugio, and DeLong, S. E. (1979) Abyssal tholeiites from the Oceanographer Fracture Zone II. Phase equilibria and mixing. Contributions to Mineralogy and Petrology, 70, 111–125.

Walker, David, Kirkpatrick, R. J., Longhi, John, and Hays, J. F. (1976) Crystallization history of lunar picritic basalt sample 12002: Phase-equilibria and cooling-rate studies. Geological Society of America Bulletin, 87, 646–656.

Walker, David, Powell, M. A., Lofgren, G. E., and Hays, J. F. (1978) Dynamic crystallization of a eucrite basalt. Proceedings of the 9th Lunar and Planetary Science Conference, 1369–1391.

Winkler, H. G. F. (1949) Crystallization of basaltic magma as recorded by variations of crystal size in dikes. Mineralogical Magazine, 28, 557–574.

Manuscript received, August 8, 1983;
accepted for publication, October 26, 1984.